Towards 5G wireless systems: A modified Rake receiver for UWB indoor multipath channels

Said Ghendir , Salim Sbaa , Ali Al-Sherbaz , Riadh Ajgou, Ali Chemsa

Abstract:

This paper presents a modified receiver based on the conventional Rake receiver for Ultra-Wide Band (UWB) indoor channels of femtocell systems and aims to propose a new solution to mitigate the multipath phenomenon. Furthermore, this work proposes an upgrade for the conventional Rake receiver to fulfill the needs of 5G wireless systems through a new concept named ‘‘hybrid femtocell’’ that joins UWB with millimeter wave (mmWave) signals. The modified receiver is considered to be a part of the UWB/mmWave hybrid femtocell system, where it is developed for confronting the indoor multipath channels and to ensure a flexible transmission based on an Intelligent Controlling System (ICS). Hence, we seek to exploit the circumstances when the channel is less complex to switch the transmission to a higher data rate through higher Mary Pulse Position Modulation (PPM). Furthermore, an ICS algorithm is proposed and an analytical model is developed followed by performance studies through simulation results. The results show that using the UWB technology through the modified receiver in femtocells could aid in mitigating the multipath effects and ensuring high throughputs. Thus, the UWB based system promotes Internet of Things (IoT) devices in indoor multipath channels of future 5G.

1. Introduction

5G technology is considered a key technology that could offer a new digital world through enabling immense information exchanges at a high data rate between devices, sensors and Mobile Stations (MS). There are two views towards this technology; evolutionary and revolutionary. The evolutionary view in which this work is conducted aims to progressively evolve the existing 4G technology into 5G [1,2]. The future generation is intended to consist of heterogeneous wireless networks especially in indoor channels, such as houses, firms, workplaces, etc. Hence, it is instrumental to pursue ways to pair IoT devices with 5G cellular networks [3–5].

The motivation for this work issued from a challenging compromise between two factors; on one hand the use, of broadband spectrum offers high throughputs and leads to pair massive Machine-Type Communications (mMTC) in indoor channels, while on the other hand, using millimeter wave (mmWave) signals in such channel types generates dense multipath components [6–15]; this is because the wavelengths of these signals are very close to the dimensions of small indoor obstacles, such as screws, buttons, pen heads, etc.

As a novelty, we aim to involve the UWB technology of 4G as a substitute candidate to respond to the above-mentioned challenge and fill the gap of mmWave signals in indoor channels. Thus, in view of the availability of reasonable broadband spectrum of UWB signals and their centimeter waves (cmWave), such signals can prove to be a middle solution between pairing a massive number of devices in high throughput and retaining the ability to face the multipath fading channel. Furthermore, since UWB technology can be

used for short-range communication systems with low power consumption (in the order of milliwatt), and due to its large bandwidth (in the order of giga hertz) that offers a huge throughput (in the order of giga bps), we decided to involve UWB besides mmWave in femtocells as an appropriate solution, thereby forming what we named ''UWB/mmWave hybrid femtocell''. In order to ensure an in-depth study of this hybrid femtocell, we restricted our study to developing a modified receiver based on the conventional Rake receiver for UWB/mmWave hybrid femtocells. We hope to continue studying other parts belonging to hybrid femtocells in future studies.

The contributions constituting this work can be summarized in the following points:

- Proposing an intelligent controlling system (ICS) algorithm to confront the UWB multipath channel.
- Offering a new adaptive modulation technique not only based on the SNR changes, but also based on multipath changes. This matter is usually neglected in previous works.
- Developing an analytical model according to the modified receiver.

In related works, many researches have investigated the problem of multipath channels [16–21] and several techniques have been proposed to deal with the multipath phenomenon. The authors in [16] have proposed a channel estimation scheme based on advanced mmWave lens antenna arrays. This scheme can be used for time-division-duplexing or frequency-division-duplexing estimations in order to minimize the number of radio-frequency (RF) chains. In [17], the authors have dealt with performance degradation due to indoor multipath channels in the next generation. They have proposed programmable wireless environments based on a new paradigm to control and mitigate the multipath fading, which is defined by given software. Two techniques were investigated in [18] for interference mitigation in multicell 5G, fractional frequency reuse (FFR) and soft frequency reuse (SFR), where Rayleigh fading channel was assumed over log-normal shadowing. The authors in [19,20] were interested in the channel estimation, where the UWB system performance was analyzed through the conventional Rake receiver. In [21], the authors have proposed an adaptive Rake receiver that uses received signals to evaluate the channel parameters based on Bayesian theory.

2. System architecture and UWB signals

Under the spotlight of the UWB/mmWave hybrid femtocell addressed in the introduction, Fig. 1 describes the global architecture showing the hybrid femtocell with the coexisting cells (mmWave small cell, mmWave base station (BS)). The use of UWB signals in hybrid femtocells allows facing the multipath problem because UWB are characterized by cmWave signals rather than mmWave signals investigated in the literatures [6–10,15,16]. This matter helps to better confront multipath channels due to signal wavelength compared with obstacles' dimensions.

As a scenario, we depicted ''a house'' in Fig. 1 so as to present an indoor multipath channel, where different IoT devices such as (virtual reality device, Camera, tablet computer, etc.) and mobile user are covered by UWB signals, whereas mmWave signals are only used to intercommunicate data with BS. In such environment, there are numerous obstacles with small sizes (in the order of millimeter). Also, when we use mmWave signals, dense multipath will be generated and this could conduct to a communication outage between all devices and hybrid access point. Furthermore, when the user moves, the case will be more complicated because the multipath will change as well. Hence, in our study we took into account the multipath changes in femtocell conjointly with SNR changes, where this matter was not addressed before.

Currently, the development of UWB technology standards for indoor uses and objects tracking are intended with the future IEEE 802.15.4z (4z) standard, where the official publication is expected at the end of 2019

[22]. Besides, the process of beamforming adopted by several researches in 5G is difficult to be implemented in mmWave BS. This is due to the fact that focusing the waves transmitted by BS precisely towards tens of hundreds of MS and IoT devices is impossible. This issue represents a great loss and a non-identical distribution of energy in the environment. For that reason, it is suggested to use the beamforming process only towards the indoor femtocell and outdoor small cell antennas, while maintaining the beamforming and positioning of surrounding devices for the mentioned sub-cells. Hence, UWB technology could play a useful role in femtocells, and promote 5G wireless network through many reasons, confronting multipath, allowing high throughput, offering high-definition positioning for which UWB signals are very appropriate [23].

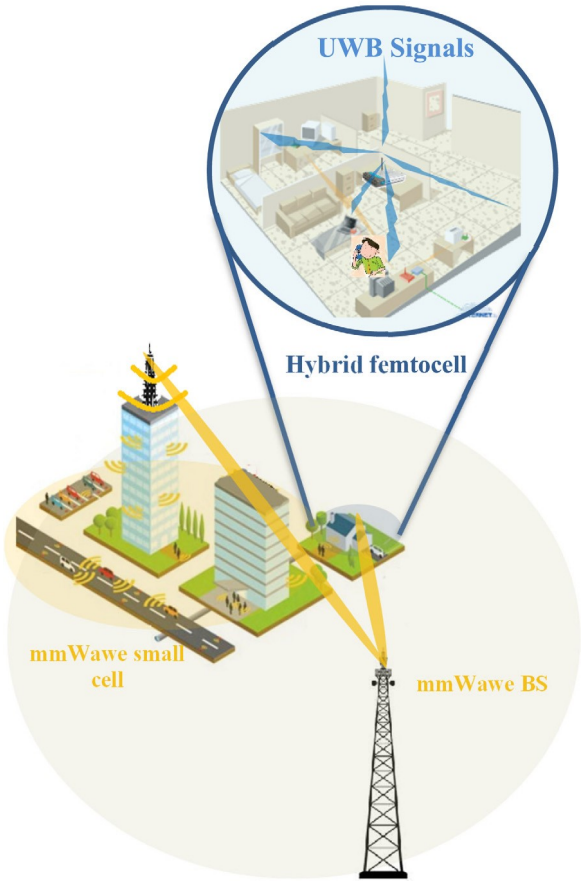

Fig. 1. General system architecture including the hybrid femtocell.

The UWB signal in our work is constructed through the Time Hopping TH-UWB structure with M-ary PPM, where the PPM modulation is based on delaying the impulse in order to distinguish between binary data, Hence, the UWB signal structure can be given by [20,24]

$$s^n(t) = \sum_{k=-\infty}^{+\infty} \sqrt{E_w^n}\, b(t - kN_f T_f - \delta \cdot (a_k^n)_{10}) \qquad (1)$$

where $b(t)$ represents information data and can be written by

$$b(t) = \sum_{j=0}^{N_f-1} w(t - jT_f - c_j^n(j)T_c)$$

E_w^n is the impulse energy from user n, $w(t)$ is the impulse shape whose energy is normalized to one, each symbol duration T_s is divided into equally-spaced N_f frames with duration T_f, where $T_s = N_f T_f = 1/R_s$ and R_s is the binary symbol rate. The sequence c_j^n is the Time Hopping Code (THC) associated with the desired user in the jth frame and it is between {0, N_c −1}. N_c is a number of chips in one frame, the parameter T_c is the duration of the chip, δ is the time shift difference that represents the modulation factor for M-ary and $(a_k^n)_{10}$ is the kth transmitted binary symbol for a desired user n, taken in the decimal representation ($0 \le (a_k^n)_{10} \le M - 1$).

We have chosen the first derivative of a Gaussian impulse which is the monocycle impulse. The basic Gaussian waveform is given by [25]

$$w_0(t) = \varepsilon \exp\left[-2\pi \left(\frac{t}{t_p}\right)^2\right] \qquad (2)$$

where t_p is the effective half width of the impulse $w_0(t)$, and ε is introduced for normalization reasons.

The n-order monocycle is

$$w_n(t) = \varepsilon_n \frac{d^n}{dt^n}\left[\exp\left(-2\pi \left(\frac{t}{t_p}\right)^2\right)\right] \qquad (3)$$

The autocorrelation function for any n is

$$R_n(\Delta) \triangleq \int_{-\infty}^{+\infty} w_n(t) w_n(t - \Delta)\mathrm{d}t = (-1)^n \frac{d^{(2n)}(R_0(\Delta))}{d\Delta^{(2n)}} \qquad (4)$$

where

$$R_0(\Delta) = \varepsilon_0^2 \frac{t_p}{2} \exp\left(-\pi \left(\frac{\Delta}{t_p}\right)^2\right)$$

From (2) the Gaussian monocycle $w_1(t)$ in time domain can be defined as

$$w_1(t) = \varepsilon_1 \frac{-4\pi t}{t_p^2} \exp\left[-2\pi \left(\frac{t}{t_p}\right)^2\right] \qquad (5)$$

The autocorrelation function of the Gaussian monocycle is

$$R_1(\Delta) = \varepsilon_1^2 \frac{\pi}{t_p}\left(1 - 2\pi \left(\frac{\Delta}{t_p}\right)^2\right) \exp\left(-\pi \left(\frac{\Delta}{t_p}\right)^2\right) \qquad (6)$$

To normalize the energy of impulse we choose

$$\varepsilon_1 = \sqrt{t_p/\pi}$$

Fig. 2 shows the structure of the M-ary PPM TH scheme for 2 and 4 PPM as an example.

The PPM modulation is founded on delaying the monocycle impulse by a modulation factor δ to obtain the transmitted data. For 2 PPM, we use one delay of δ to differentiate between ''0'' and ''1'', while for 4PPM, we use four delays of δ to differentiate between ''00'', ''01'', ''10'' and ''11''.

The transmitted throughput is $log_2 M$, where $M = 2^{g+1}$ and g is the modulation level $g = 0,... G$.

To find out the maximum level G of M-ary PPM modulation that can be involved in the scheme, the following relation must be verified

$$(2)^{G+1} 2t_p \leq T_c \Rightarrow G \leq \log_2\left(\frac{T_c}{2t_p}\right) - 1 \qquad (7)$$

That implies

$$G \leq \log_2\left(\frac{\rho}{N_c}\right) - 1 \qquad (8)$$

where the spreading ratio is expressed as $\rho = T_f / 2t_p$

3. Modified Rake receiver

Fig. 3 shows the generic blocks of the modified Rake receive, which is based on the conventional Rake receiver [20,26,27], and is placed in order to coherently collect the determined multiple paths through different procedures, such as correlators, channel estimation and combining operations. Moreover, these correlators use template signals with the same time hopping codes as the ones used by the transmitter.

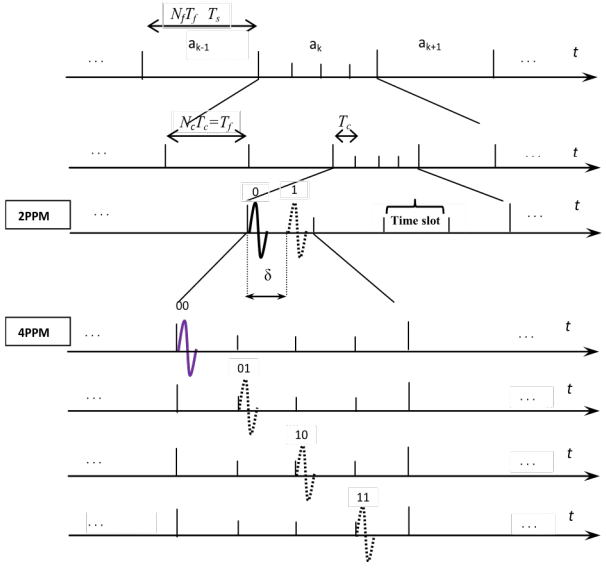

Fig. 2. Structure of the M-ary PPM time hopping scheme for $M = 2, 4$.

On the other hand, as a contribution made to the conventional Rake receiver to reach best performances in the midst of the challenges of future 5G wireless systems, our strategy uses an ICS that includes three main blocks that are a Channel Model (CM) Classifier, an Automatic Switcher and a Controlling process. Furthermore, by considering the conventional Rake receiver as a hand consisting of different fingers allocated for L paths, our the modified Rake receiver can be viewed as a Rake receiver backed up by a number of hands depending on the number of time slots i pre-assigned for symbols a_k. Furthermore, the above-mentioned

hands work simultaneously in parallel, thereby making the acquisition of symbols as rapid as possible, where each hand has a template signal $m_i(t)$ allocated for the M-ary PPM modulation level.

Additionally, to make the CM classifier able to select channel models from the predefined classes, it would be better to subdivide the UWB channel into different models. In this regard, we exploit the existing channel models based on the modified Saleh– Valenzuela model [28] that has been modified and adopted by the IEEE 802.15.3a [29] by taking into account the clustering phenomena observed in several UWB channel measurements [30]. Therefore, four different channel models are defined CM1, CM2, CM3, and CM4.

Fig. 4 describes the flowchart of the proposed ICS algorithm. In the following, we describe the different blocks by the steps listed below:

Step 1: It is the channel estimation, where before starting the communication between the transmitter and the receiver, the parameters α_l and τ_l are unknown a priori and must be estimated by a simple and quick method as in [20], where the authors have proposed UWB channel estimation, based on the maximum-likelihood criterion.

Step 2: which is the channel classification, where the CMclassifier seeks the closest model to the estimated channel models (from CMs: CM1-4). The CM classier is based on a simpler parameter called the mean delay of propagation τ_m corresponding to the gravity center of each channel model (τ_{1m}, τ_{2m}, τ_{3m} and τ_{4m}). These mean delays are obtained from the many measurements discussed in [31] and related to IEEE.802.15.3a channel models. Thus, the CM classier keeps comparing the mean delays with the mean delay $\tilde{\tau}_m$ of the estimated channel models.

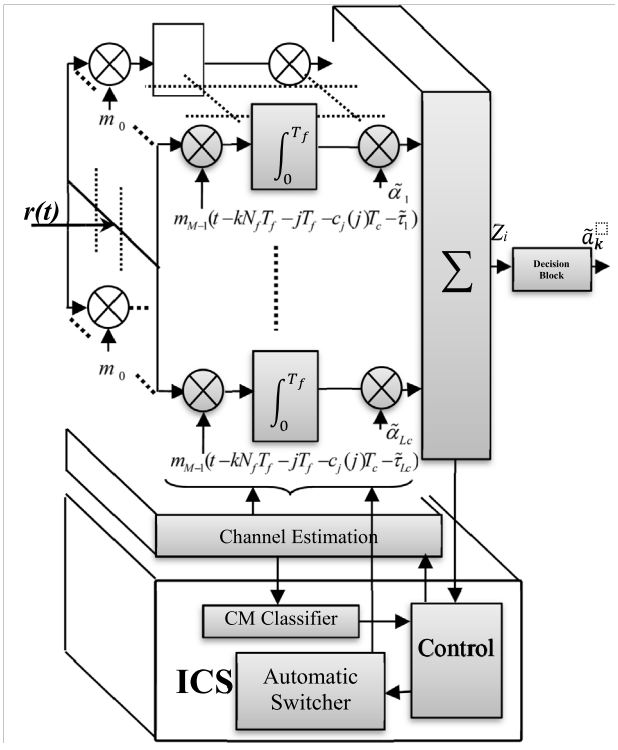

Fig. 3. Generic blocks for the proposed receiver.

Step 3: It is the outage checking. The first check is the conditions under which the system may declare an outage, where each channel model has a pre-defined SNR threshold x_{g^*} (CMs) allocated for the modulation level g. The outage probability P_{out} is the probability that the mean SNR x falls below the minimum threshold SNR x_{0^*} (CMs) corresponding to the target probability of bit error P_{b^*}; when the system falls in such case, it would declare an outage and start re-estimating the channel to allocate the adequate modulation level; when x is not sufficient to guarantee the target probability of bit error, no bits are transmitted and the communication is in outage until other conditions.

Step 4: It is the automatic switching, where when the model is selected, the ICS will adapt the appropriate modulation level on both the transmitter/receiver; thereby the Automatic Switcher changes the modulation to the selected level. For that, if x exceeds or drops below the SNR threshold x_{g^*} (CMs) designed for the modulation level g, the throughput can be increased or decreased by increasing or decreasing the modulation level between $g = 0$ and g_{max} allocated for the chosen channel, where g_{max} does not necessarily mean G as it will be discussed in the performance evaluation.

Step 5: It is the decision. This step checks the combining processes over each hand by comparing the energy Z_a of time slot a (whose the symbol currently received is $a_k{-}_1$) corresponding to the active hand, with the energies Z_i of time slots i carried by the other hands. If one of these hands gets a higher energy during the transmission than the active hand, the corresponding symbol a_k of the new time slot is considered as received.

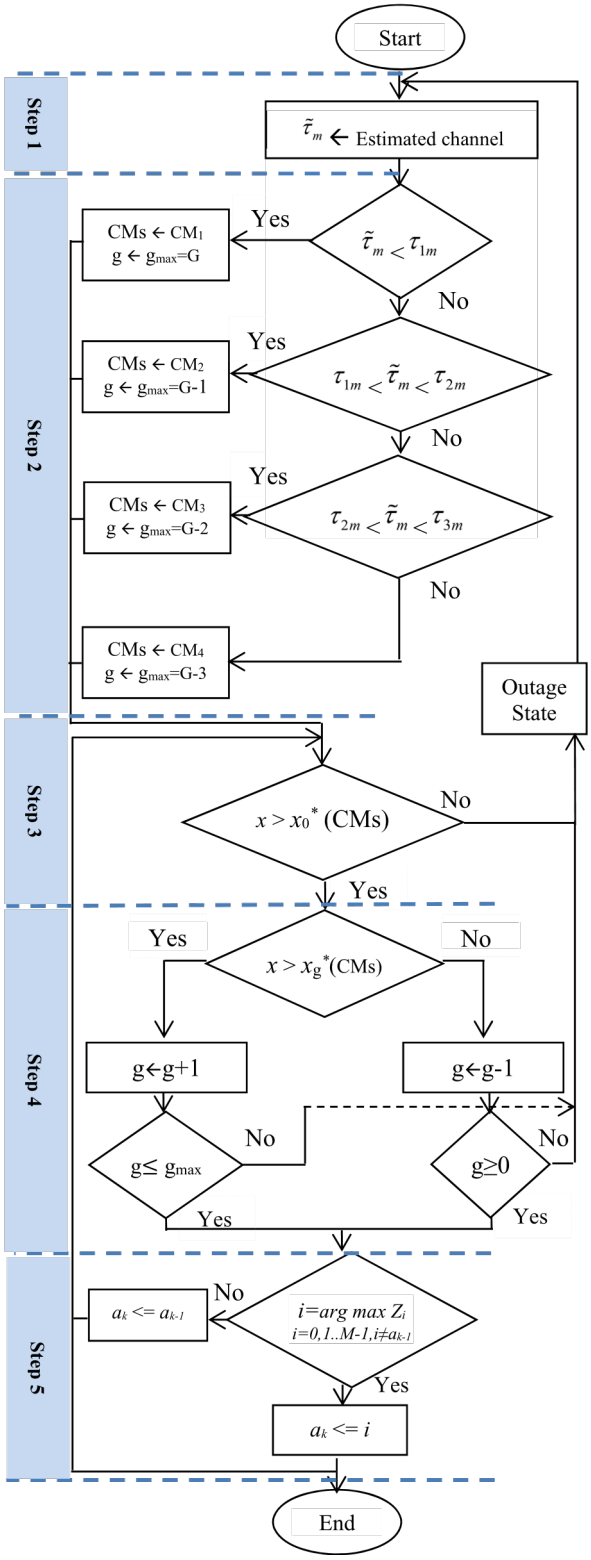

Fig. 4. Flowchart of the proposed ICS Algorithm.

The UWB signals are transmitted over a multipath channel with *L* paths with the presence of the AWGN, the channel can be represented as

$$h(t) = \sum_{l=1}^{L} \alpha_l (t - \tau_l) + n(t) \tag{9}$$

The received signal specified for all users can be written as

$$r^n(t) = \sum_{n=1}^{Nu} \sum_{l=1}^{L} \alpha_l^n s^n (t - \tau_l^n) + n(t) \tag{10}$$

The parameter α_l^n is the channel attenuation that follows lognormal distribution [20], and . τ_l^n is the relative time delay of the lth path of the received signal associated with user n. Furthermore, $n(t)$ is zero-mean AWGN with power spectral density
$N_0/2$.

The signal at the receiver for a desired user can be given by

$$r(t) = \sqrt{E_w} \sum_{k=-\infty}^{+\infty} \sum_{j=0}^{N_f - 1} \sum_{l=1}^{L} \alpha_l w(t - kN_f T_f - jT_f - c_j(j)T_c - \delta a_k - \tau_l) + n(t) \tag{11}$$

Obviously, the receiver has fingers less than the independent fading paths $L_c < L$. Furthermore, the received signal is integrated over a period corresponding to one frame duration. The weighted sum of the correlators is subsequently applied to a detector that determines the transmitted symbol $\widetilde{a}_k$ for a desired user.

4. Performance analysis

We perform the system performance analysis considering that the receiver is interested only in the desired user. Moreover, it is interesting to note that only the effects of Inter-Symbol/Frame Interference (*ISFI*) and the *AWGN* are considered here. The UWB channel can be considered as a linear system according to the superposition principle; thus instead of studying the channel effect for a composite signal with several symbols, we are interested in studying the channel effects for only one symbol sent by the transmitter. Moreover, by applying the same principle for the frames in one symbol, $s(t)$ can be expressed for one frame as

$$s(t) = \sqrt{E_w} w(t - cT_c - \delta \cdot a) \tag{12}$$

where c represents the time code specific to the concerned frame and a is the transmitted binary symbol represented in decimal number.

The received signal is given by

$$r(t) = \sqrt{E_w} \sum_{l=1}^{Lc} \alpha_l w(t - cT - \delta \cdot a - \tau_l) + n(t) \tag{13}$$

L_c characterizes the number of the receiver fingers, which is less than the independent fading paths $L_c < L$

The decision statistic Z_i specific to the energy of the ith time slot within a duration T_c is the maximal-ratio combination of the outputs of the correlators, this is because each ith time slot is ensured by gathering all receiver fingers so as to maximize the resulted energy. Hence, decision statistic is given by the following expression

$$Z_i = \sum_{l=1}^{Lc} \tilde{\alpha}_l \int_{jT_f}^{(j+1)T_f} r(t) m_i(t - jT_f - c_j(j)T_c - \tilde{\tau}_l) dt \tag{14}$$

$$Z_i = \sum_{l'=1}^{Lc} \tilde{\alpha}_{l'} \int_{0}^{T_f} r(t) m_i(t - cT_c - \tilde{\tau}_{l'}) dt \tag{15}$$

The template signals have the following formula

$$m_i(t) = w(t - \delta \cdot i) \quad (i = 0, 1, \ldots M - 1) \tag{16}$$

From (16) and (13), we can deduce

$$Z_i = \sqrt{E_w} \sum_{l'=1}^{Lc} \sum_{l=1}^{Lc} \tilde{\alpha}_{l'} \alpha_l \int_{0}^{T_f} w(t - cT_c - \delta \cdot a - \tau_l) \cdot w(t - cT_c - \delta \cdot i - \tilde{\tau}_{l'}) dt + \int_{0}^{T_f} n(t) \left(\sum_{l'=1}^{Lc} \tilde{\alpha}_{l'} \cdot w(t - cT_c - \delta \cdot i - \tilde{\tau}_{l'}) \right) dt \tag{17}$$

$$Z_i = \sqrt{E_w} \sum_{l'=1}^{Lc} \sum_{l=1}^{Lc} \tilde{\alpha}_{l'} \alpha_l R_w(\Delta) + N \tag{18}$$

$R_w(\Delta)$ is the correlation function of the Gaussian monocycle $w(t)$, and is given by

$$R_w(\Delta) = \int_{0}^{T_f} w(t) w(t - \Delta) dt \tag{19}$$

$$\Delta = \delta \cdot (i - a) + (\tilde{\tau}_{l'} - \tau_l) \tag{20.a}$$

Δ is the time difference between the different paths and the different time slots from the ath time slot. Furthermore, it is assumed that Δ is a uniformly distributed random variable over the duration T_f.

In the remainder of this study, without loss of generality and in an attempt to reach simplified and more controllable formulas, the received attenuations α will be considered equal to the estimated attenuations $\tilde{\alpha}$, and at the same time, the estimated delays $\tilde{\tau}$ will be considered equal to the received delays τ. Under these conditions (20.a) becomes

$$\Delta = \delta \cdot (i - a) + (\tau_{l'} - \tau_l) \tag{20.b}$$

In order to get the binary symbol a, Z_i must be maximized by

$$\Delta = 0 \Leftrightarrow (i = a \wedge l = l') \tag{21}$$

Hence, Z_i can be written as

$$Z_i = \left(\sqrt{E_w} \sum_{l=1}^{Lc} \tilde{\alpha}_l^2 \right) \cdot \delta_{i-a} + ISFI + N \tag{22}$$

where δ_{i-a} is the Kronecker delta.

$$\delta_{i-a} = \begin{cases} 0, & if\ i \neq a \\ 1, & i = a \end{cases}$$

For this reason, Z_i can be given by

$$Z_i = A \cdot \delta_{i-a} + ISFI + N \tag{23}$$

where A is the desired energy allocated for the unknown symbol $\tilde{a}_i$ and obtained when $\Delta = 0$, where A is expressed as

$$A = \sqrt{E_w} \sum_{l=1}^{Lc} \tilde{\alpha}_l^2 \tag{24}$$

ISFI is the self-interference due to the multipath channel

$$ISFI = \sqrt{E_w} \sum_{l'=1}^{Lc} \sum_{l=1}^{Lc} \tilde{\alpha}_{l'} \tilde{\alpha}_l R_w(\Delta) \Big|_{\Delta \neq 0} \tag{25}$$

N is *AWGN* component at the output receiver, and is expressed as

$$N = \int_0^{T_f} n(t) \left(\sum_{l'=1}^{Lc} \tilde{\alpha}_{l'} \cdot w(t - cT_c - \delta \cdot i - \tilde{\tau}_{l'}) \right) dt \tag{26}$$

From (6), the normalized autocorrelation function is

$$R_w(\Delta) = (1 - 2\pi \left(\frac{\Delta}{t_p} \right)^2) \exp \left(-\pi \left(\frac{\Delta}{t_p} \right)^2 \right) \tag{27}$$

$R_w(\Delta)$ in particular cases can be expressed as

$$R_w(\Delta) = \begin{cases} 1, & \Delta = 0 \\ 0, & |\Delta| \geq T_f \end{cases} \tag{28}$$

The mean of $R_w(\Delta)$ is given by

$$E\left[R_w(\Delta)\right] = \int_{-2t_p}^{2t_p} R_w(\Delta)\frac{1}{2T_f}d\Delta \tag{29}$$

The 2nd moment of $R_w(\Delta)$ is given by

$$E\left[R_w^2(\Delta)\right] = 2\int_{0}^{2t_p} R_w^2(\Delta)\frac{1}{2T_f}d\Delta \tag{30}$$

After some calculus we obtain

$$E\left[R_w(\Delta)\right] = \frac{3.4873 \cdot 10^{-6}}{\rho}$$

$$E\left[R_w^2(\Delta\tau)\right] = \frac{0.0442}{\rho}$$

By considering the signals as being transmitted in the ath time slot, the decision variables Z_i can be subdivided into two main subsets

$$Z_i = \begin{cases} Z_a: A + ISFI + N, & i = \mathrm{a} \\ Z_{\bar{a}}: ISFI + N, & i = 0, \ldots, \mathrm{M}-1, \mathrm{i} \neq a \end{cases} \tag{31}$$

where, Z_a represents the desired energy quantity in which the signal is transmitted in the ath time slot, Z_a^- represents the undesired energy quantity.

However, given that the UWB multipath channel has a large number of paths and according to applying the central limit theorem, we can consider the *ISFI* follows a Gaussian distribution. Hence, the decision variables are as follows

$$\begin{aligned} Z_a &\sim \ Normal\left(A + E\left[ISFI\right] + E\left[N\right],\ \sigma_{ISFI}^2 + Var\ (N)\right) \\ Z_{\bar{a}} &\sim \ Normal\left(E\left[ISFI\right] + E\left[N\right],\ \sigma_{ISFI}^2 + Var\ (N)\right) \end{aligned} \tag{32}$$

$E[N]$ and $Var(N)$ are found to be 0 and $N_0/2$ respectively.

The Eq. (25) can be written as

$$ISFI = \left(\sqrt{E_w}\sum_{l'=1}^{Lc}\sum_{l=1}^{Lc}\tilde{\alpha}_{l'}\tilde{\alpha}_l R_w(\Delta) - A\cdot\delta_{i-a}\right) \tag{33}$$

$$E\left[ISFI\right] = \sqrt{E_w}\frac{3.4873\cdot 10^{-6}}{\rho}\sum_{l'=1}^{Lc}\sum_{l=1}^{Lc}\tilde{\alpha}_{l'}\tilde{\alpha}_l - A\cdot\delta_{i-a} \tag{34}$$

We write $ISFI^2$ as follows to find out σ_{ISFI}^2

$$\begin{aligned} ISFI^2 = E_w\cdot\sum_{l'''=1}^{Lc}\sum_{l''=1}^{Lc}\sum_{l'=1}^{Lc}\sum_{l=1}^{Lc}\tilde{\alpha}_{l'''}\tilde{\alpha}_{l''}\tilde{\alpha}_{l'}\tilde{\alpha}_l R_w(\Delta')\cdot R_w(\Delta) \\ -\ 2\sqrt{E_w}A\sum_{l'=1}^{Lc}\sum_{l=1}^{Lc}\tilde{\alpha}_{l'}\tilde{\alpha}_l R_w(\Delta)\cdot\delta_{i-a} + A^2\cdot\delta_{i-a}\Big) \end{aligned} \tag{35}$$

where, $\Delta = \delta\cdot(i-a) + (\tau_{l'} - \tau_l)$, and $\Delta' = \delta\cdot(i-a) + (\tau_{l'''} - \tau_{l''})$

It is known that $\sigma_{ISFI}^2 = E\left[ISFI^2\right] - E\left[ISFI\right]^2$ therefore

$$\begin{aligned} \sigma_{ISFI}^2 = E_w\cdot\Bigg(\sum_{l'''=1}^{Lc}\sum_{l''=1}^{Lc}\sum_{l'=1}^{Lc}\sum_{l=1}^{Lc}\tilde{\alpha}_{l'''}\tilde{\alpha}_{l''}\tilde{\alpha}_{l'}\tilde{\alpha}_l\cdot E\left[R_w(\Delta')\cdot R_w(\Delta)\right] \\ -\sum_{l'''=1}^{Lc}\sum_{l''=1}^{Lc}\sum_{l'=1}^{Lc}\sum_{l=1}^{Lc}\tilde{\alpha}_{l'''}\tilde{\alpha}_{l''}\tilde{\alpha}_{l'}\tilde{\alpha}_l\cdot E\left[R_w(\Delta)\right]^2\Bigg) \end{aligned} \tag{36}$$

Knowing that $E\left[R_w(\Delta')\cdot R_w(\Delta)\right] = E\left[R_w(\Delta)\right]^2$ if $\Delta \neq \Delta'$, we obtain

$$\sigma_{ISFI}^2 = E_w \cdot \left(\frac{12.1613\cdot 10^{-12}}{\rho^2} \sum_{l'''=1}^{Lc}\sum_{l''=1}^{Lc}\sum_{l'=1}^{Lc}\sum_{l=1}^{Lc} \tilde{\alpha}_{l'''}\tilde{\alpha}_{l''}\tilde{\alpha}_{l'}\tilde{\alpha}_{l} \Big|_{\Delta\neq\Delta'} + \frac{0.0442}{\rho} \sum_{l'''=1}^{Lc}\sum_{l''=1}^{Lc}\sum_{l'=1}^{Lc}\sum_{l=1}^{Lc} \tilde{\alpha}_{l'''}\tilde{\alpha}_{l''}\tilde{\alpha}_{l'}\tilde{\alpha}_{l} \Big|_{\Delta=\Delta'} - \frac{12.1613\cdot 10^{-12}}{\rho^2} \sum_{l'''=1}^{Lc}\sum_{l''=1}^{Lc}\sum_{l'=1}^{Lc}\sum_{l=1}^{Lc} \tilde{\alpha}_{l'''}\tilde{\alpha}_{l''}\tilde{\alpha}_{l'}\tilde{\alpha}_{l} \right) \tag{37}$$

The probability density function (pdf) of the desired energy part can be written as

$$p\left(Z_a\right) = \frac{1}{\sqrt{2\pi}\sigma} e^{-\frac{(Z_a-\mu_a)^2}{2\sigma^2}} \tag{38}$$

where, $\mu_a = A + E\left[ISFI\right]$ and $\sigma = \sqrt{\sigma_{ISFI}^2 + \frac{N_0}{2}}$

The pdf of the undesired energy part can be written as

$$p\left(Z_{\bar{a}}\right) = \frac{1}{\sqrt{2\pi}\sigma} e^{-\frac{(Z_{\bar{a}}-\mu_{\bar{a}})^2}{2\sigma^2}} \tag{39}$$

where, $\mu_{\tilde{a}} = E\,[ISFI]$

The conditional probability of correct decision is

$$P_C = prob(Z_a > Z_1, \ldots, Z_a > Z_i, \ldots, Z_a > Z_M \mid Z_a, \quad i \neq a) \quad (40)$$

Hence,

$$P_C = \int_{-\infty}^{\infty} [prob(Z_a > Z_i) \mid Z_a, \quad i \neq a]^{M-1}\, p(Z_a) dZ_a \quad (41)$$

By substituting (38) and (39) into (41), and after some calculus we get

$$P_C = \frac{1}{\sqrt{\pi} 2^{M-1}} \int_{-\infty}^{\infty} \left[1 + erf\left(x + \frac{A}{\sqrt{2}\sigma}\right)\right]^{M-1} e^{-x^2} dx \quad (42)$$

where, $x = \frac{Z_a - \mu_a}{\sqrt{2}\sigma}$

The average probability can be found by averaging the conditional probability of the correct decision over the probability density function (pdf) $f(\xi)$, where $\xi = \sum_{l=1}^{Lc} \tilde{\alpha}_l^2$ represents the received energy collected by the L_c fingers of the receiver, and is described as the sum of lognormal random variables (RVs) and follows the pdf $f(\xi)$ as indicated in [32].

$$\overline{P}_c = \int_0^{\infty} P_c(\xi).f(\xi) d\varepsilon \quad (43)$$

To evaluate the UWB system performance through M-ary PPM, we use the probability of bit error given by [33]

$$P_b = \frac{M \cdot P_s}{2(M-1)} = \frac{M(1 - \overline{P}_c)}{2(M-1)} \quad (44)$$

where $P_s = 1 - \overline{P}_c$ is the probability of symbol.

We take the case of the slow adaptive modulation process towards the channel changes, taking $x_g{}^*$ as the minimum SNR threshold required for the gth modulation level to guarantee the target probability of bit error (target BER) $P_b{}^*$ i.e., $P_b(x_g{}^*) = P_b{}^*$. Thus the outage probability that is the probability that the probability of bit error P_b is greater than the target probability of bit error [32] is given by

$$P_{out}\left(P_b{}^*\right) = \mathbb{P}\left\{P_b\,(x) > P_b{}^*\right\} = F_x\left(x_0^*\right) \quad (45)$$

$F_x(\cdot)$ is the cumulative density function (CDF) of the mean SNR parameter x and is expressed as

$$F_x\left(x_g{}^*\right) = Q\left(\frac{Z_a - \mu_a}{\sqrt{2}\sigma}\right) \tag{46}$$

where $Q(.)$ is the Gaussian-Q function.

x may up-cross or down-cross the SNR threshold x^* to increase or decrease the throughput respectively. Then the mean throughput can be given by [34]

$$\begin{aligned} V &= \sum_{g=0}^{G-1}(g+1)\mathbb{P}\left\{x_g{}^* < x \le x_{g+1}^*\right\} + (G+1)\mathbb{P}\left\{x_G^* < x\right\} \\ &= \sum_{g=0}^{G-1}(g+1)\left[F_x\left(x_{g+1}^*\right) - F_x\left(x_g{}^*\right)\right] + (G+1)\left[1 - F_x\left(x_G^*\right)\right] \end{aligned} \tag{47}$$

5. Performance evaluation

In this section, the simulations are performed to show the performance of the modified receiver. All results have been obtained using Matlab simulations for one user. The sampling frequency f_c = 30 GHz; the binary symbol rate R_s = 300 Mbps, the signal bandwidth is 11.5 GHz and the center frequency is 7 GHz. The number of frames per symbol and the duration of one frame are respectively N_f = 1 and T_f = 3.33 ns, where each impulse occupies one frame; the number of chips in one frame and the duration of one chip are respectively N_c = 2, T_c = 1.66 ns; the time hopping code c_j = {1}; the modulation factor δ = 0.1 ns, and the impulse duration $2t_p$ = 0.2 ns that implies that the spreading ratio ρ = 33.3 and the maximum modulation level G = 3, i.e. $M_{\max}$ = 16. The estimation sequence length is 100 symbols. Regarding the paths, we have adopted the same notion of S-Rake type, where only the number of paths that have undergone 10 dB of attenuation compared to the strongest path have been considered.

Fig. 5(a), (b), (c) and (d) presents the performance evaluation of the BER versus E_b/N_0 for channel models (CM1, CM2, CM3 and CM4), where the different modulations 2, 4, 8 and 16-ary PPM have been assessed. It is clearly shown that the agreement between simulation and analytical results is excellent where the BER increases as we apply higher-level modulation.

According to the philosophy of the suggested strategy, the ICS switches to the modulation level by considering the classified model chosen by the CM classifier. Furthermore, by taking the target probability of bit error $P_b{}^* = 10^{-4}$, the following can be judged:

First, when the estimated channel is classified as CM1, then the ICS switches to 16-ary PPM ($g = G = 3$) through the
Automatic Switcher according to our algorithm. This situation corresponds to Fig. 5. (a). Hence, we could take $x_3{}^*$(CM1) = 22 dB as SNR threshold for the level g = 3;

1. If the mean SNR x drops below $x_3{}^*$(CM1), then 8-ary PPM (g = 2) is adopted automatically; the SNR threshold in this case drops down to $x_2^{*(\mathrm{CM1})} = 20$ dB (please see CM1 in Fig. 5(b)).

2. If *x* drops below 20 dB, then 4-ary PPM (*g* = 1) is adopted automatically; the SNR threshold in this case drops down to $x_1^{*(\mathrm{CM1})} = 18$ dB (please see CM1 in Fig. 5(c)).
3. If *x* drops below 18 dB, then 2-ary PPM (*g* = 0) is adopted automatically; the SNR threshold in this case drops down to $x_0{}^*$(CM1) = 16.5 dB (please see CM1 in Fig. 5(d)).

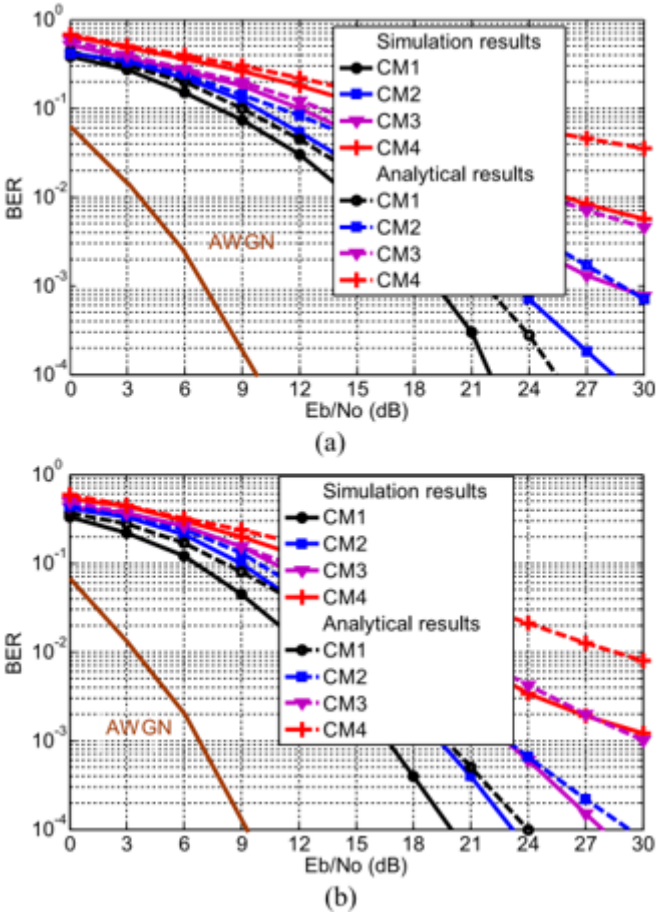

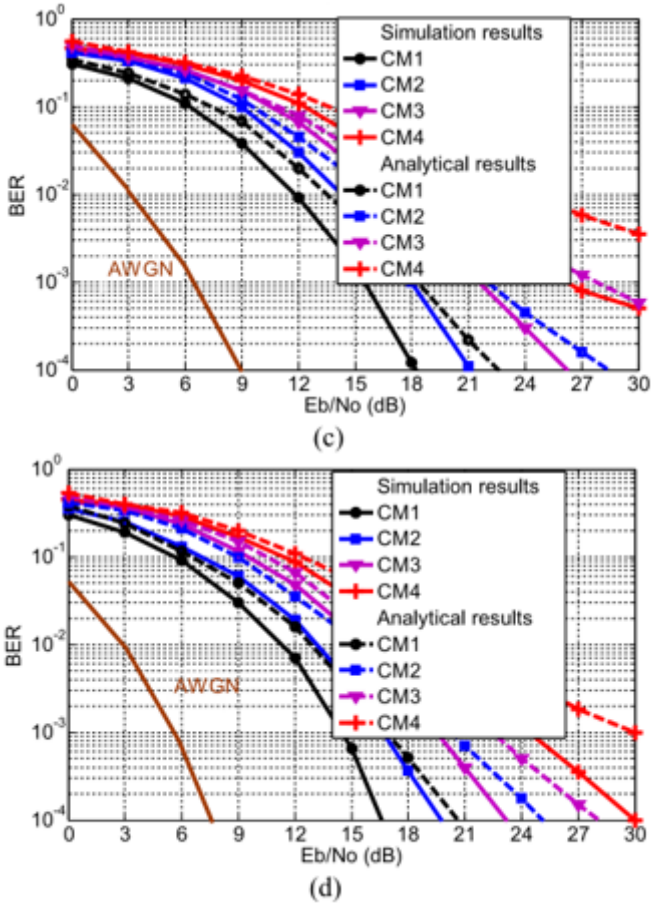

Fig. 5. BER evaluation versus E_b/N_0 for the proposed receiver, σ = 6 dB, μ_a = 2 dB: (a) 16-ary PPM. (b) 8-ary PPM. (c) 4-ary PPM. (d) 2-ary PPM.

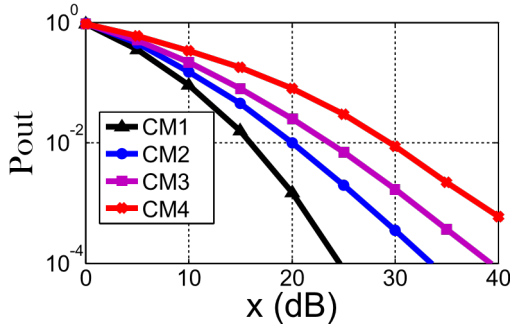

Fig. 6. P_{out} versus the mean SNR x, $P_b^* = 10^{-4}$, σ = 6 dB, μ_a = 2 dB.

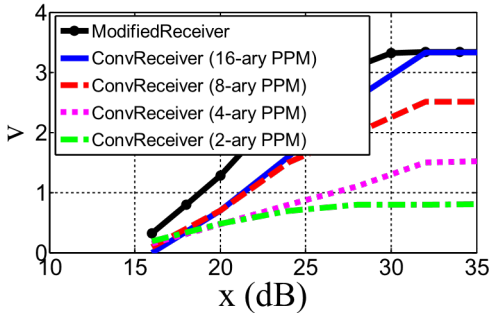

Fig. 7. Throughput versus the mean SNR *x*

- For the modified Rake receiver: $P_b^* = 10^{-4}$, $\sigma = 6$ dB, $\mu_a = 2$ dB, maximum outage probability 1% for all models
- For the conventional Rake receiver with separate cases of modulations (16-ary PPM, 8-ary PPM, 4-ary PPM and 2-ary PPM).

4. If *x* drops below $x_0^{*(\mathrm{CM1})} = 16.5$ dB, the ICS declares an outage and starts re-estimating the channel to allocate an adequate modulation level.
5. If *x* in any previous case exceeds the above-mentioned SNR thresholds of modulation levels *g*, then the level *g* + 1 would be adopted until reaching the maximum level $g_{\max} = G = 3$ where we get the maximum throughput for CM1.

Second, when the estimated channel is classified as CM2, then the ICS switches to 8-ary PPM according to our algorithm. This situation corresponds to Fig. 5(b); thereby, we can take $x_2^{*(\mathrm{CM2})} = 23$ dB as the SNR threshold for the level *g* = 2;

1. If the mean SNR *x* drops below $x_2^{*(\mathrm{CM2})} = 23$ dB, then
   4-ary PPM (*g* = 1) is adopted automatically; the SNR threshold in this case drops down to $x_1^{*(\mathrm{CM2})} = 21$ dB (please see CM2 in Fig. 5(c)).
2. If *x* drops below $x_1^{*(\mathrm{CM2})} = 21$ dB, then 2-ary PPM (g=0) is adopted automatically; the SNR threshold in this case drops down to x_0^* (CM2) = 19.5 dB (please see CM2 in Fig. 5(d)).
3. If *x* drops below x_0^* (CM2) = 19.5 dB, the ICS declares an outage and starts re-estimating the channel to allocate an adequate modulation level.
4. If *x* in any of the previous case exceeds the above-mentioned SNR thresholds of modulation levels *g*, then the level *g* + 1 is adopted until reaching the maximum allowable level $g_{\max} = 2$ for CM2.

Third, when the estimated channel is classified as CM3, then according to our algorithm the ICS switches to 4-ary PPM. This situation corresponds to Fig. 5(c). Therefore, we can take $x_1^{*(\mathrm{CM3})} = 26$ dB as the SNR threshold for the level *g* = 1;

1. If the mean SNR *x* drops below x_1^*(CM3), then g=0 is adopted automatically; the SNR threshold in this case drops down to $x_0^{*(\mathrm{CM3})} = 23$ dB (please see CM3 Fig. 5(d)).
2. If *x* drops below $x_0^{*(\mathrm{CM3})} = 23$ dB, the ICS declares an outage and starts re-estimating the channel to allocate again an adequate modulation level.
3. If *x* in any of the previous case exceeds the above-mentioned SNR thresholds of modulation levels *g*, then the level *g* + 1 is adopted until reaching the maximum allowable level $g_{\max} = 1$ for CM3.

Fourth, when the estimated channel is classified as CM4, it is characterized by a huge number of paths. Then according to our algorithm the ICS switches to 2-ary PPM or stops the transmission completely until other conditions, this situation corresponds to
Fig. 5(d), where we can take $x_0^{*(CM4)} = 30$ dB as the minimum threshold SNR allocated for the lowest modulation level $g = 0$; if the mean SNR x drops below x_0^* (CM4), the ICS declares an outage and starts re-estimating the channel.

Furthermore, the outage probability of all the models is evaluated in Fig. 6, where the maximum outage probability is found to be 1% by taking the previous minimum thresholds that yield a target probability of bit error of 10^{-4}, i.e. x_0^* (CM1) = 16.5 dB, $x_0^{*(CM2)} = 19.5$ dB, $x_0^{*(CM3)} = 23$ dB, $x_0^{*(CM4)} = 30$ dB.
Moreover, the time occupation considered for CM1, CM2, CM3 and CM4 are 50%, 38%, 07%, 05% respectively. Regarding the mean throughput, we made a comparison in Fig. 7 between the modified Rake receiver and the conventional Rake receiver with separate cases of modulations (16-ary PPM, 8-ary PPM, 4-ary PPM, 2-ary PPM).

Finally, as we have observed from Fig. 7, the obtained throughput by the modified receiver gives better performance than the conventional one [20] especially in low mean SNR values. Moreover, unlike the research work given by [17] where they defined the multipath by software before mitigating them, which can delay the transmission processes, this work deals instantaneously with the multipath phenomenon. The results and the above discussion prove that the circumstance when the channel is less complex can be exploited so as to switch the transmission to a higher throughput by going through to higher-level modulations while using classified models.

6. Conclusion

This work investigated a future challenge that 5G will face, which is the negative multipath effect caused by the mmWave signals in indoor channels. As a solution, we proposed the use of UWB technology conjointly with mmWave femtocells. Thus, we developed a modified Rake receiver that belongs to the hybrid femtocell. ICS algorithm was developed to ensure an adaptive modulation by following a multipath with SNR changes simultaneously. Furthermore, this receiver upgraded the conventional Rake receiver to meet the future requirements of 5G wireless systems in indoor channels (low energy consumption, high throughput, flexible transmission and adaptive modulation). Finally, the achieved throughput in the midst of multipath challenges is quite sufficient to promote the use of the modified receiver to be used in a hybrid femtocell of the 5G wireless systems.

Declaration of competing interest

The authors declare that they have no known competing financial interests or personal relationships that could have appeared to influence the work reported in this paper.

References

[1] E. Ezhilarasan, M. Dinakaran, A review on mobile technologies: 3G, 4G and 5G, in: 2017 Second International Conference on Recent Trends and Challenges in Computational Models, ICRTCCM, Tindivanam, 2017, pp. 369–373.

[2] S. Onoe, 1.3 evolution of 5G mobile technology toward 1 2020 and beyond, in: 2016 IEEE International Solid-State Circuits Conference, ISSCC, San Francisco, CA, 2016, pp. 23–28.

[3] S. Singh, N. Saxena, A. Roy, H. Kim, A survey on 5G network technologies from social perspective, IETE Tech. Rev. 34 (1) (2017) 30–39.

[4] Al-Turjman Fadi, 5G-enabled devices and smart-spaces in social-IoT: an overview, Future Gener. Comput. Syst. 92 (2019) 732–744.

[5] T. Qiu, N. Chen, K. Li, M. Atiquzzaman, W. Zhao, How can heterogeneous Internet of Things build our future: A survey, IEEE Commun. Surv. Tutor. 20 (3) (2018) 2011–2027.

[6] J. Huang, Y. Liu, C. Wang, J. Sun, H. Xiao, 5G millimeter wave channel sounders, measurements, and models: Recent developments and future challenges, IEEE Commun. Mag. 57 (1) (2019) 138–145.

[7] A.S.A. Mubarak, H. Esmaiel, E.M. Mohamed, Efficient mm wave link establishment and maintaining using Wi-Fi/mm wave interworking, in: 2018 International Conference on Computing, Electronics & Communications Engineering, iCCECE, Southend, United Kingdom, 2018, pp. 220–225.

[8] P. Zhang, J. Li, H. Wang, H. Wang, W. Hong, Indoor small-scale spatiotemporal propagation characteristics at multiple millimeter-wave bands, IEEE Antennas Wirel. Propag. Lett. 17 (12) (2018) 2250–2254.

[9] S. Salous, et al., Millimeter-wave propagation: Characterization and modeling toward fifth-generation systems. [Wireless Corner], IEEE Antennas Propag. Mag. 58 (6) (2016) 115–127.

[10] T.S. Rappaport, G.R. MacCartney, M.K. Samimi, S. Sun, Wideband millimeter-wave propagation measurements and channel models for future wireless communication system design, IEEE Trans. Commun. 63 (9) (2015) 3029–3056.

[11] J. Ghosh, D.N.K. Jayakody, M. Qaraqe, Downlink capacity of OFDMA-CR based 5G femtocell networks, Phys. Commun. (2018).

[12] K. Saito, J. Takada, M. Kim, Dense multipath component characteristics in 11-GHz-band indoor environments, IEEE Trans. Antennas and Propagation 65 (9) (2017) 4780–4789.

[13] Z. Jakó, J. Ghosh, Network throughput and outage analysis in a Poisson and Matérn cluster based LTE-advanced small cell networks, AEU-Int. J. Electron. Commun. 75 (2017) 46–52.

[14] Joydev Ghosh, Dushantha Nalin K. Jayakody, Game theoretic frequency reuse approach in OFDMA femtocell networks, Trans. Emerg. Telecommun. Technol. (2018).

[15] B. Soleimani, M. Sabbaghian, Cluster-based resource allocation and user association in mmWave femtocell networks, IEEE Trans. Commun. (2018) http://dx.doi.org/10.1109/TCOMM.2018.2881464.

[16] L. Yang, Y. Zeng, R. Zhang, Channel estimation for millimeter-wave MIMO communications with lens antenna arrays, IEEE Trans. Veh. Technol. 67 (4) (2018) 3239–3251.

[17] Christos Liaskos, Nie Shuai, Ageliki Tsioliaridou, et al., A novel communication paradigm for high capacity and security via programmable indoor wireless environments in next generation wireless systems, Ad Hoc Netw. 87 (2019) 1–16.

[18] Joydev Ghosh, Dushantha Nalin K. Jayakody, An analytical view of ASE for multi-cell OFDMA networks based on frequency reuse scheme, IEEE Syst. J. (2018).
[19] H. Sheng, A.M. Haimovich, Impact of channel estimation on ultra-wideband system design, IEEE J. Sel. Top. Sign. Proces. 1 (3) (2007) 498–507.
[20] V. Lottici, A. D'Andrea, U. Mengali, Channel estimation for ultra-wideband communications, IEEE J. Sel. Areas Commun. 20 (9) (2002) 1638–1645.
[21] M. Wang, Y. Han, W. Sheng, A Bayesian approach to adaptive RAKE receiver, IEEE Access 6 (2018) 3648–3654.
[22] http://www.ieee802.org/15/pub/TG4z.html, 28.02.2019.
[23] A.A. Adebomehin, S.D. Walker, Enhanced ultrawideband methods for 5G LOS sufficient positioning and mitigation, in: 2016 IEEE 17th International Symposium on A World of Wireless, Mobile and Multimedia Networks, WoWMoM, Coimbra, 2016, pp. 1–4.
[24] M.Z. Win, R.A. Scholtz, Ultra-wide bandwidth time-hopping spreadspectrum impulse radio for wireless multiple-access communications, IEEE Trans. Commun. 48 (4) (2000) 679–689.
[25] T. Zhang, T.D. Abhayapala, R.A. Kennedy, Performance of ultra-wideband correlator receiver using Gaussian monocycles, in: Communications, 2003 ICC '03 IEEE International Conference on, vol. 3, 2003, pp. 2192–2196.
[26] G.L. Turin, Introduction to spread-spectrum antimultipath techniques and their application to urban digital radio, Proc. IEEE 68 (3) (1980) 328–353.
[27] D. Cassioli, F. Vatalaro, M.Z. Win, A.F. Molisch, Performance of lowcomplexity rake reception in a realistic UWB channel, in: Proc. IEEE Int. Conf. Commun, vol. 2, 2002, pp. 763–767.
[28] A.A.M. Saleh, R. Valenzuela, A statistical model for indoor multipath propagation, IEEE J. Sel. Areas Commun. 5 (2) (1987) 128–137.
[29] A.F. Molisch, J.R. Foerster, M. Pendergrass, Channel models for ultrawideband personal area networks, IEEE Wirel. Commun. 10 (6) (2003) 14–21.
[30] J. Kunisch, J. Pamp, Measurement results and modeling aspects for the UWB radio channel, in: 2002 IEEE Conference on Ultra Wideband Systems and Technologies, IEEE Cat. No.02EX580, Baltimore, MD, USA, 2002, pp. 19–23.
[31] J.R. Foerster, M. Pendergrass, A.F. Molisch, A channel model for ultra wideband indoor communication, in: International Symposium on Wireless Personal Multimedia Communications, WPMC, 2003.
[32] L.C. Wang, W.C. Liu, Bit error rate analysis in IEEE 802.15.3a UWB channels, IEEE Trans. Wirel. Commun. 9 (5) (2010) 1537–1542.
[33] J.G. Proakis, Digital Communications, third ed., McGraw-Hill, 1995.
[34] A. Conti, M.Z. Win, M. Chiani, Slow adaptive M-QAM with diversity in fast fading and shadowing, IEEE Trans. Commun. 55 (5) (2007) 895–905.